Macromolecules

ARTICLE

pubs.acs.org/Macromolecules

Dielectric and Viscoelastic Investigation of Segmental Dynamics of Polystyrene above Glass Transition Temperature: Cooperative Sequence Length and Relaxation Mode Distribution

Yumi Matsumiya, Akiko Uno, and Hiroshi Watanabe*

Institute for Chemical Research, Kyoto University, Uji, Kyoto 611-0011, Japan

Tadashi Inoue and Osamu Urakawa

Department of Macromolecular Science, Osaka University, Toyonaka, Osaka 560-0043, Japan

ABSTRACT: Atactic polystyrene (PS) has the type-B dipole perpendicular to the chain backbone so that its local, segmental motion activates the dielectric relaxation. For monodisperse oligostyrene (OS) and PS samples of various molecular weights M, details of this motion were examined at temperatures T well above T_g through comparison of the complex modulus, $G^* = G' + iG''$, and the complex dielectric permittivity, $\varepsilon^* = \varepsilon' - i\varepsilon''$, measured as functions of the angular frequency ω. For the OS samples, $G^*(\omega)$ and $\varepsilon^*(\omega)$ fully relaxed through the segmental dynamics thereby exhibiting respective terminal relaxation tails (low-frequency tails), $G'(\omega) \propto \omega^2$, $G''(\omega) \propto \omega$, $\Delta\varepsilon'(\omega) \equiv \varepsilon'(0) - \varepsilon'(\omega) \propto \omega^2$, and $\varepsilon''(\omega) \propto \omega$, at ω below the segmental relaxation frequency ω_s. For the PS samples, $G^*(\omega)$ relaxed partly through the segmental dynamics and then exhibited the polymeric full relaxation characterized by the Rouse-like behavior followed by the terminal flow behavior (with/without intermediate entanglement plateau depending on M). In contrast, $\varepsilon^*(\omega)$ of the PS samples still relaxed completely through the segmental dynamics. For respective samples, the $G^*(\omega)$ and $\varepsilon^*(\omega)$ data in the segmental relaxation zone exhibited very similar relaxation mode distribution and had the same time−temperature shift factor. Nevertheless, a ratio of the dielectrically and viscoelastically detected segmental relaxation times, $r(M) = \omega_{s,G}/\omega_{s,\varepsilon}$, and the dielectric relaxation intensity, $\Delta\varepsilon(M)$, decreased with increasing M up to $M^* \cong 2 \times 10^3$ and then became insensitive to M on a further increase of M. The viscoelastic segmental relaxation reflects the cooperative torsion of the repeating units along the molecular backbone (as noted from rheo-optical data), while the dielectric segmental relaxation detects reorientational motion of those units affected by both intra- and intermolecular cooperativity (as noted from the basic dielectric expression). The observed decreases of $r(M)$ and $\Delta\varepsilon(M)$ suggested that the dimension ξ_m of the whole OS molecule (over which the cooperative torsion occurs) is smaller than the length scale ξ_c for the intermolecular cooperative motion and that ξ_m approaches ξ_c on an increase of M up to M^*. Consequently, the high-M PS molecules having $\xi_m > \xi_c$ exhibited the M-insensitive $r(M)$ and $\Delta\varepsilon(M)$. Thus, the M value for the crossover between these two regimes, $M^* \cong 2 \times 10^3$, can be taken as the molecular weight of the cooperative sequence along the PS backbone. Furthermore, the quantitative similarity of the viscoelastic and dielectric mode distributions suggests that the cooperative torsion of the repeating units along the molecular backbone is governed by the cross-correlation of the units belonging to different molecules.

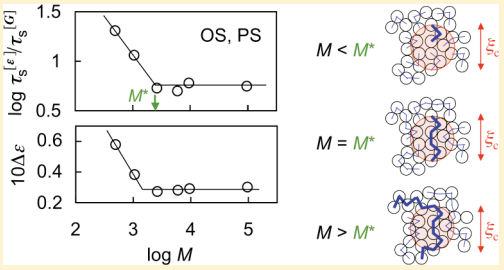

1. INTRODUCTION

For atactic (noncrystalline) homopolymers, the local motion, or the "segmental" motion, is activated on an increase of temperature T above the glass transition temperature T_g. Thus, the segmental dynamics is intimately related to the glass transition and has been investigated extensively from both experimental and theoretical aspects.[1−21] In the current molecular picture, the repeating units of polymers exhibit both inter- and intrachain cooperative motion and the glass transition occurs when a length scale of this cooperativity increases above a threshold value on a decrease of T. Although the cooperative region corresponding to this length scale has not been detected with direct methods such as scattering,[13] this molecular picture is in harmony with the viscoelastic (mechanical), dielectric, NMR, and thermal data so far accumulated: The mode broadening of the segmental relaxation process (thermo-rheological complexity) in a close vicinity of T_g, noted in the viscoelastic, dielectric, and NMR measurements,[1−4,7−12,17,18,20,21] can be attributed to changes of the cooperativity length scale and the dynamic heterogeneity[21] with T (that result in a change of the motional modes of the repeating units). The aging/rejuvenation[14−16] detected with the dielectric and other methods can be related to a time evolution of this scale in a nonequilibrium state.

Received: March 19, 2011
Revised: April 24, 2011
Published: May 03, 2011

Table 1. Characteristics of Samples[a]

sample code	$10^{-3}M_w$	M_w/M_n	T_g/°C[b]
OS-0.5	0.49_5	1.14	−44
OS-1	1.0_5	1.13	7
OS-3	2.6_3	1.05	58
PS-6	5.9_7	1.02	80
PS-10	9.5_0	1.02	90
PS-96	$96._4$	1.05	92

[a] Supplied from Tosoh. [b] Temperature at the onset of endothermic behavior determined with DSC.

The broadening of the segmental dynamics explained above is observed only in the close vicinity of T_g and vanishes at T well above T_g.[21] The segmental relaxation process becomes thermorheologically simple to have a T-insensitive mode distribution at such high T, and the time−temperature shift factor a_T of this process approaches a_T for the terminal relaxation process,[2,11,12,20] the latter reflecting the global motion of the polymer chains over a length scale comparable to the chain dimension. In this high-T zone, the spatial scale of the motional cooperativity of the repeating units becomes insensitive to T thereby giving this simplicity. The segmental relaxation is believed to correspond to the cooperative, torsional motion of a sequence of ∼10 repeating units in the chain backbone. Nevertheless, to the best knowledge of the authors, no quantitative experimental test has been made for this hypothesis at T well above T_g.

Thus, we attempted to make this test through comparison of linear viscoelastic and dielectric data of atactic polystyrene (PS) samples of various molecular weights M (including oligomers with $M < 3000$). PS has the type-B dipole[12,22,23] perpendicular to the chain backbone so that its segmental motion activates the dielectric relaxation. The comparison revealed that a ratio of the dielectrically and viscoelastically detected segmental relaxation times, $r(M) = \tau_s^{[\varepsilon]}/\tau_s^{[G]}$, and the dielectric relaxation intensity, $\Delta\varepsilon(M)$, decreased with increasing M up to $M^* \cong 2 \times 10^3$ and then became insensitive to M on a further increase of M. The viscoelastic segmental relaxation detects cooperative, intramolecular torsion of the repeating units along the molecular backbone[24−26] while the dielectric segmental relaxation reflects reorientational motion of those units affected by both intra- and intermolecular cooperativity.[12,22,23,27−30] Considering this molecular origin of the viscoelastic and dielectric relaxation, we may relate the decreases of $r(M)$ and $\Delta\varepsilon(M)$ seen for $M < M^*$ to a situation that the molecular size is smaller than the length scale ξ_c for the intermolecular cooperativity, and the M-insensitive $r(M)$ and $\Delta\varepsilon(M)$ for $M > M^*$, to the opposite situation. Thus, $M^* \cong 2 \times 10^3$ can be taken as the molecular weight of the cooperative sequence having strong cross-correlation in the backbone of the polymeric molecule (PS). Furthermore, the similarity of the viscoelastic and dielectric mode distributions suggests that the cooperative torsional dynamics is essentially determined by the cross-correlation of the repeating units belonging to different molecules. Details of these results are presented in this paper.

2. EXPERIMENTAL SECTION

2.1. Materials. Commercially available oligostyrene (OS) and polystyrene (PS) samples (TSK's, Tosoh Co.) were utilized. Table 1 summarizes molecular characteristics of these samples. The sample code number indicates the molecular weight in unit of 1000. All samples, in particular those with $M \geq 2.6\times 10^3$, had a narrow molecular weight distribution.

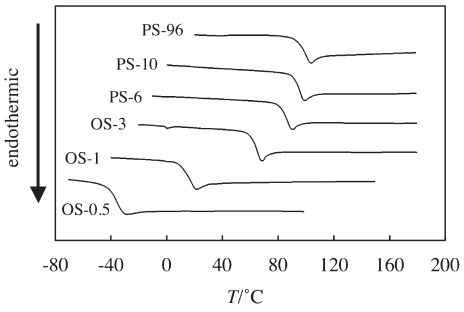

Figure 1. DSC traces of OS and PS samples as indicated.

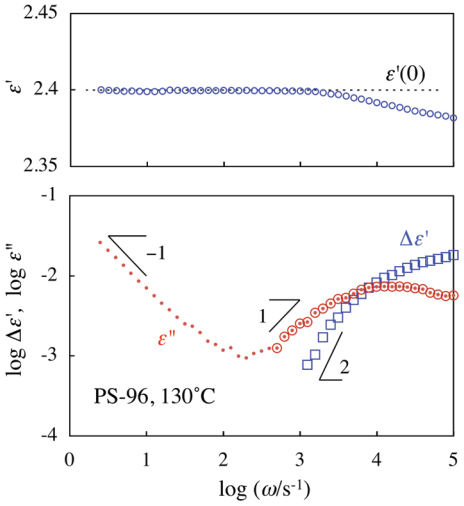

Figure 2. Dielectric behavior of PS-96 sample at 130 °C.

The samples were subjected to dielectric and viscoelastic measurements. For removal of ionic impurities, each sample was dissolved in cyclohexane (guaranteed grade, Wako Co.) at a concentration of ∼0.2 wt % and kept quiescently overnight in a glass beaker that was freshly cleaned with a phosphorus-free alkaline detergent (Scat 20X-PF, Nacalai Tesque Co.), thoroughly rinsed with distilled and ion-exchanged water, and dried (baked) at ∼120 °C for 4 h and then cooled just prior to use. After this overnight storing, the solution was slowly sucked out from the beaker into a freshly cleaned and baked eggplant glass flask and concentrated up to 10−30 wt % under reduced pressure. Finally, the concentrated solution was transferred to another freshly cleaned and baked glass beaker and freeze-dried in vacuum at room temperature and then thoroughly dried in high vacuum at ∼90 °C. The OS and PS samples purified in this way exhibited very low direct current (dc) conduction even at high T (>100 °C) possibly because most of ionic impurities were adsorbed on the clean glass wall of the beaker and eggplant flask. Those samples exhibited the terminal dielectric relaxation behavior at intermediate to high frequencies without being disturbed by the dc conduction, as shown later in Figures 2 and 3.

2.1. Measurements. For the OS and PS bulk samples listed in Table 1, differential scanning calorimetric (DSC) measurements were conducted with a laboratory calorimeter (Q20; TA Instruments). The results are shown in Figure 1. The heating rate was 10 °C min^{-1}. In this study, the glass transition temperature T_g was evaluated as the temperature at the onset of endothermic behavior. The T_g values thus obtained are summarized in Table 1.

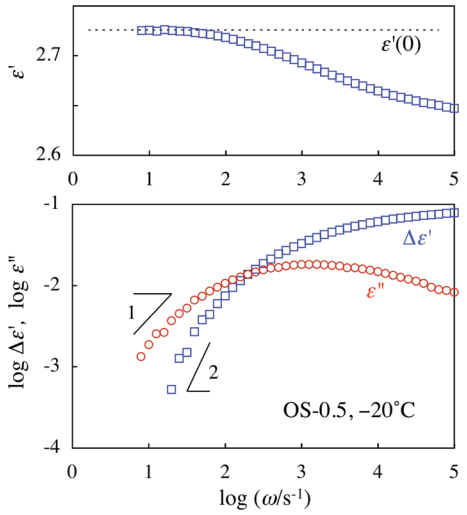

Figure 3. Dielectric behavior of OS-0.5 sample at −20 °C.

Dynamic viscoelastic and dielectric measurements were conducted for those samples with a laboratory rheometer (ARES; TA Instruments) and an impedance analyzer/dielectric interface system (1260 and 1296, Solartron), respectively. A parallel-plate fixture (diameter = 4 mm) and a parallel-plate dielectric cell with a guard electrode (vacant capacitance = 20 pF) were utilized in respective measurements. For each sample, the measurement was made at temperatures $T > T_g + 5$ (mainly in a range of $T_g + 10 < T < T_g + 30$). The viscoelastically and dielectrically detected segmental relaxation process was thermo-rheologically simple at those T.

3. RESULTS

3.1. Overview of Viscoelastic and Dielectric Behavior. For the OS and PS samples listed in Table 1, the dielectric measurements were conducted at several temperatures $T/°C > T_g + 5$ without being too much disturbed by the dc conduction. As an example, Figures 2 and 3 show the angular frequency (ω) dependence of the dynamic dielectric constant $\varepsilon'(\omega)$, its decrease from the static dielectric constant, $\Delta\varepsilon'(\omega) \equiv \varepsilon'(0) - \varepsilon'(\omega)$, and the dielectric loss $\varepsilon''(\omega)$, measured for the PS-96 and OS-0.5 samples (the highest-M and lowest-M samples examined) at +130 and −20 °C, respectively. The dielectric relaxation seen for these samples is attributed to the segmental dynamics that activates fluctuation of the type-B dipoles.

Within the framework of the linear stimulus-response theory, $\Delta\varepsilon'(\omega)$ and $\varepsilon''(\omega)$ are expressed in terms of the dielectric relaxation spectrum $\{g_p, \tau_{\varepsilon,p}\}$ as[23,31,32]

$$\Delta\varepsilon'(\omega) = \Delta\varepsilon \sum_p g_p \frac{\omega^2 {\tau_{\varepsilon,p}}^2}{1 + \omega^2 {\tau_{\varepsilon,p}}^2}$$

$$\varepsilon''(\omega) = \Delta\varepsilon \sum_p g_p \frac{\omega\tau_{\varepsilon,p}}{1 + \omega^2 {\tau_{\varepsilon,p}}^2} \quad (1a)$$

with

$$\sum_p g_p = 1 \quad (1b)$$

Here, $\tau_{\varepsilon,p}$ and g_p indicate the characteristic time and normalized intensity of pth dielectric relaxation mode, and $\Delta\varepsilon$ is the total dielectric relaxation intensity. As noted from eq 1a, completion of the relaxation at $\omega < 1/\tau_{\varepsilon,1}$ (with $\tau_{\varepsilon,1}$ = longest dielectric relaxation time) is unequivocally characterized by the power-law type terminal relaxation tails (low-frequency tails) of $\Delta\varepsilon'(\omega)$ and $\varepsilon''(\omega)$,

$$\Delta\varepsilon'(\omega) \propto \omega^2, \quad \varepsilon''(\omega) \propto \omega \quad (\text{at } \omega < 1/\tau_{\varepsilon,1}) \quad (2)$$

These tails are clearly observed in Figures 2 and 3. (The terminal relaxation tail of $\varepsilon''(\omega)$ is noted also for a remarkable set of dielectric data for PS as well as polydimethylsiloxane reported by Hintermeyer and co-workers.[33]) The terminal dielectric relaxation time (second-moment average relaxation time), $\langle\tau_\varepsilon\rangle$, is evaluated from the $\Delta\varepsilon'(\omega)$ and $\varepsilon''(\omega)$ data in the terminal tail regime as[23]

$$\langle\tau_\varepsilon\rangle \equiv \frac{\sum_p g_p {\tau_{\varepsilon,p}}^2}{\sum_p g_p \tau_{\varepsilon,p}} = \left[\frac{\Delta\varepsilon'}{\omega\varepsilon''}\right]_{\omega \to 0} \quad (3)$$

Here, we should point out that the dc conduction due to ionic impurities often disturbs the observation of the terminal relaxation

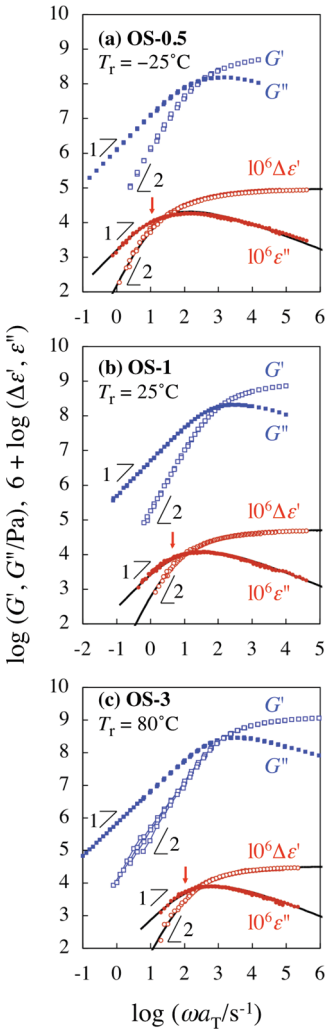

Figure 4. Master curves of the viscoelastic and dielectric data for OS samples with $M < 3 \times 10^3$. The dielectric $\Delta\varepsilon'$ and ε'' data are multiplied by a factor of 10^6. The arrows attached to the dielectric data indicates the relaxation frequency $1/\langle\tau_\varepsilon\rangle$ evaluated from the terminal relaxation tails of those data, and the solid curves, $\Delta\varepsilon'$ and ε'' recalculated from the KWW fitting function. For further details, see text.

dx.doi.org/10.1021/ma200631p |*Macromolecules* 2011, 44, 4355–4365

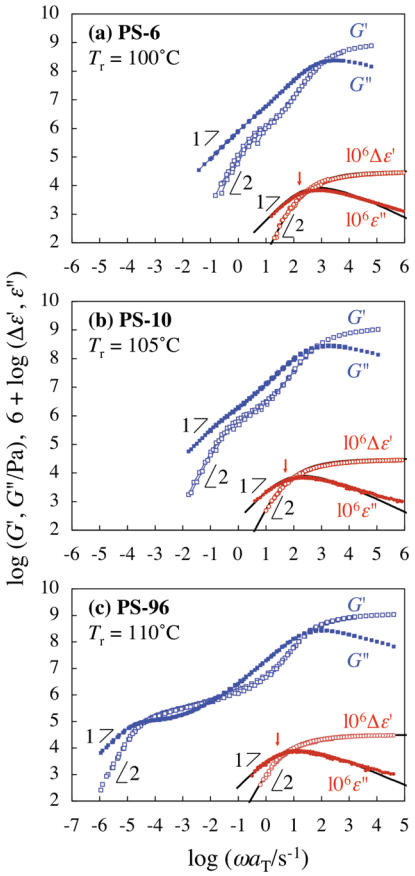

Figure 5. Master curves of the viscoelastic and dielectric data for PS samples with $M > 5 \times 10^3$. The dielectric $\Delta\varepsilon'$ and ε'' data are multiplied by a factor of 10^6. The arrows attached to the dielectric data indicates the relaxation frequency $1/\langle\tau_\varepsilon\rangle$ evaluated from the terminal relaxation tails of those data, and the solid curves, $\Delta\varepsilon'$ and ε'' recalculated from the KWW fitting function. For further details, see text.

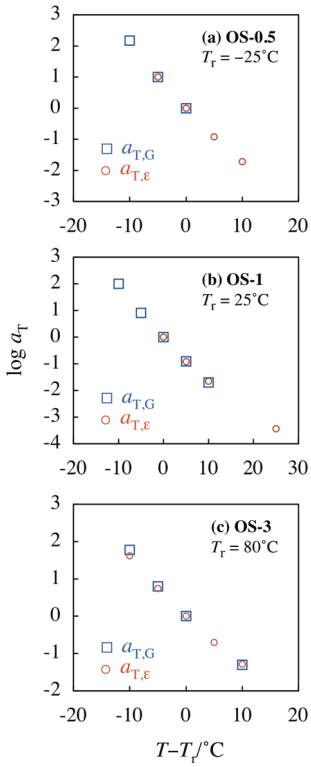

Figure 6. Shift factors $a_{T,G}$ and $a_{T,\varepsilon}$ for the viscoelastic and dielectric data of OS samples as indicated.

tails of $\Delta\varepsilon'(\omega)$ and $\varepsilon''(\omega)$ at high T. In fact, the dc conduction characterized by a relationship, $\varepsilon'' \propto \omega^{-1}$ at low ω, is noted for the PS-96 sample at 130 °C; see Figure 2. However, this conduction is rather minor and does not disturb the detection of the terminal relaxation tail of $\varepsilon''(\omega)$ at intermediate to high ω because this sample was purified with the method explained earlier. For the other samples having lower M, the dc conduction was even less significant and the terminal relaxation tails of $\Delta\varepsilon'(\omega)$ and $\varepsilon''(\omega)$ were observed more clearly; cf. Figure 3. In this paper, we utilize the raw dielectric data in a range of ω where the dc contribution negligibly contributes to the data (such as those shown with large circles in the bottom panel of Figure 2), analyze those data, and discuss the features of the segmental relaxation.

For the OS and PS samples with $M < 3 \times 10^3$ and $M > 5 \times 10^3$, respectively, Figures 4 and 5 examine the time−temperature superposability of the viscoelastic and dielectric data at $T > T_g + 5$ (mostly at $T > T_g + 10$). The arrows attached to the $\Delta\varepsilon'(\omega)$ and $\varepsilon''(\omega)$ data denote the dielectric relaxation frequency $1/\langle\tau_\varepsilon\rangle$ (cf. eq 3) determined from the terminal relaxation tails of those data, and the solid curves show $\Delta\varepsilon'(\omega)$ and $\varepsilon''(\omega)$ recalculated from the Kohlrausch−Williams−Watts (KWW) fitting function explained later. For respective samples, the reference temperature T_r was chosen to be around T_g+20 °C. The corresponding shift factors are summarized in Figures 6 and 7.

All samples have only type-B dipoles and thus their dielectric relaxation detects only the segmental dynamics, not the global chain dynamics. For this reason, the dielectric data are satisfactorily time−temperature superposed in the entire range of ω, as noted in Figures 4 and 5. Note that the failure of superposition due to the mode broadening, known to occur in a *close vicinity* of T_g (and often represented as a change of the Kohlrausch−Williams−Watts parameter β with T),[2,3,7,21,28,30] was not significant at the temperatures examined in this study.

The viscoelastic data are contributed not only from the segmental dynamics but also from the global dynamics *given that* the molecules in the sample have the polymeric flexibility. For the low-M OS-0.5 and OS-1 samples, the viscoelastic segmental relaxation is directly followed by the terminal flow behavior characterized by the relationship, $G' \propto \omega^2$ and $G'' \propto \omega$; see Figures 4a and 4b. Thus, the molecules in these samples hardly have the polymeric flexibility, and their viscoelastic data in the entire range of ω are dominated by the segmental dynamics thereby obeying the superposition. Correspondingly, in the range of T examined ($>T_g + 10$ in most cases), the shift factors for the viscoelastic and dielectric data, $a_{T,G}$ and $a_{T,\varepsilon}$, agree with each other; cf. Figure 6, parts a and b.

In contrast, for higher M samples, the viscoelastic segmental relaxation is followed by the Rouse-like relaxation, and further by the entanglement relaxation in the case of $M \gg$ entanglement molecular weight M_e; see Figures 4c and 5a−c. The Rouse-like and entanglement relaxation processes result from the polymeric (global) dynamics.[24−26] Since the shift factors for the segmental and polymeric dynamics are close but not in perfect agreement, the viscoelastic data of high-M samples cannot be superposed at intermediate ω where the segmental and polymeric dynamics contribute comparably to the modulus data. In Figures 4c and

dx.doi.org/10.1021/ma200631p |*Macromolecules* 2011, 44, 4355–4365

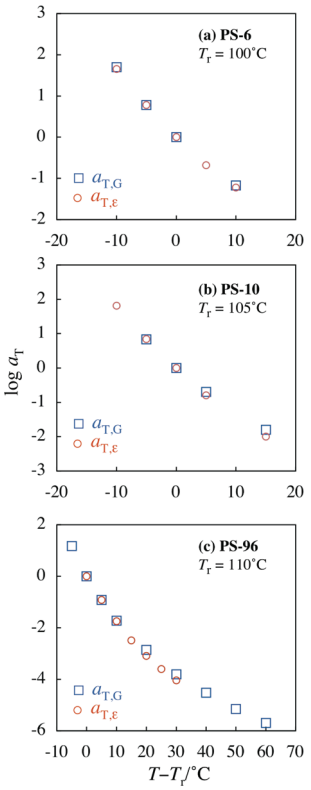

Figure 7. Shift factors $a_{T,G}$ and $a_{T,\varepsilon}$ for the viscoelastic and dielectric data of PS samples as indicated.

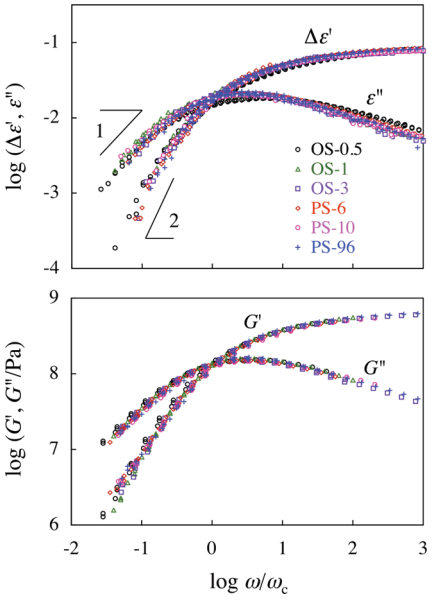

Figure 8. Comparison of the dielectric data (top panel) and viscoelastic data (bottom panel) for the segmental relaxation of OS and PS samples as indicated.

5a−c, the low-ω part of the G'' data at respective temperature was utilized as a guide for the superposition, and this method of superposition gave branches in the G' plots. (This type of failure of the superposition of the moduli data is well-known.[11,24−26] Rheo-optical analysis enables separation of those data into the segmental and polymeric contributions, although some

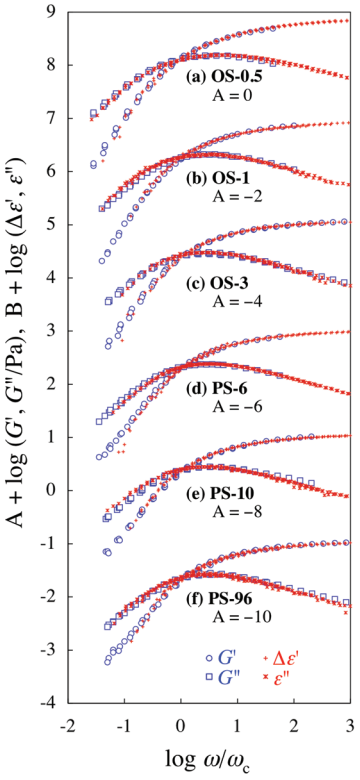

Figure 9. Comparison of the viscoelastic and dielectric mode distributions for the segmental relaxation of respective samples as indicated.

controversy may remain for the method of analysis based on the additivity of the stress and/or strain.[24−26,34−36]) Correspondingly, the difference of the shift factors for the segmental and polymeric dynamics is noted for the $a_{T,\varepsilon}$ and $a_{T,G}$ data in Figure 7, most clearly for the data of PS-96 (Figure 7c): The dielectric $a_{T,\varepsilon}$ is exclusively related to the segmental dynamics, while the viscoelastic $a_{T,G}$ is contributed from both segmental and polymeric dynamics, with the former contribution overwhelming the latter at low T. Thus, the $a_{T,\varepsilon}$ and $a_{T,G}$ data are close to each other at low T where the segmental dynamics governs both dielectric and viscoelastic data, while a deviation between $a_{T,\varepsilon}$ and $a_{T,G}$ is magnified at higher T where the viscoelastic data becomes dominated by the polymeric dynamics.

In the remaining part of this paper, we limit ourselves to the behavior in the segmental relaxation zone at low T (mainly between $T_g + 10$ and $T_g + 30$) and at high ω where the dielectric $\Delta\varepsilon^*(\omega)$ ($=\varepsilon^*(0) - \varepsilon^*(\omega)$) and viscoelastic $G^*(\omega)$ data obey the time−temperature superposition with the same a_T. Direct comparison of these $\Delta\varepsilon^*(\omega)$ and $G^*(\omega)$ data enables us to examine some details of the segmental dynamics,[37] as discussed below.

3.2. Viscoelastic and Dielectric Mode Distributions for the Segmental Relaxation. The viscoelastic and dielectric relaxation mode distributions of the OS and PS samples are observed as the ω dependence of the G', G'', $\Delta\varepsilon'$, and ε'' data. In both Figures 8 and 9, these data in the segmental relaxation zone (mainly at T between $T_g + 10$ and $T_g + 30$) are plotted against the reduced angular frequency ω/ω_c, where ω_c is the frequency at which the G' and G'' curves and/or the $\Delta\varepsilon'$ and ε'' curves cross each other. (The ω_c value is larger for the viscoelastic data than for the dielectric data, as clearly noted in Figures 4 and 5.)

dx.doi.org/10.1021/ma200631p |*Macromolecules* 2011, 44, 4355–4365

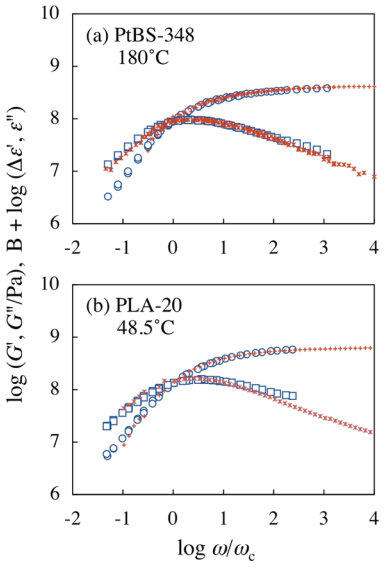

Figure 10. Comparison of the viscoelastic and dielectric mode distributions for the segmental relaxation of PtBS and PLA samples as indicated. Large circles and squares indicate the viscoelastic data, and the small plus and asterisk symbols, the dielectric data.

Changes of the mode distribution with the sample molecular weight M are examined in Figure 8 where the $\Delta\varepsilon^*$ and G^* data are separately plotted against ω/ω_c. (For the clearest comparison, the OS-0.5 sample was chosen as a reference and the $\Delta\varepsilon^*$ and G^* data of the other samples were shifted vertically in the double−logarithmic scale to match the high-ω values of $\Delta\varepsilon'$ and G' with those of the OS-0.5 sample.) For each sample, the viscoelastic and dielectric mode distributions are directly compared in Figure 9 where the G' and G'' data of respective samples are vertically shifted in the double−logarithmic scale to avoid heavy overlapping of the data points and the $\Delta\varepsilon'$ and ε'' data are further shifted to match the high-ω value of $\Delta\varepsilon'$ with that of G'.

In the top panel of Figure 8, we note that dielectric mode distribution becomes a little narrower with increasing M; compare the data for OS-0.5 and PS-96, for example. However, this change of the mode distribution with M is minor, thereby allowing all samples to exhibit the terminal relaxation tails (cf. eq 2). The changes of the viscoelastic mode distribution are also minor, as noted in the bottom panel. Thus, in the segmental relaxation zone at the temperatures examined (mainly between $T_g + 10$ and $T_g + 30$), the dielectric and viscoelastic mode distributions change only a little on the significant increase of M (from 5.0×10^2 to 9.6×10^4).

For each OS and PS sample, the viscoelastic and dielectric mode distributions in the segmental relaxation zone almost coincide with each other; see Figure 9. This quantitative similarity of the viscoelastic and dielectric mode distributions is not limited to OS and PS examined in this study but found also for the other polymer species. As an example, Figure 10 shows the plots of the literature data for the other type-B polymers, poly(*p*-*tert*-butylstyrene) (PtBS; $M = 348\times 10^3$, 180 °C)[40] and poly(lactic acid) (PLA; $M = 20 \times 10^3$, 48.5 °C),[41] reduced in the same way as in Figure 9. (PLA has both type-A and type-B dipoles, but the contribution from the former is negligible in the range of ω shown in the bottom panel of Figure 10.) The similarity of the viscoelastic and dielectric segmental mode distributions is confirmed for PtBS and PLA. The similarity was noted also for poly(vinyl ethylene) in the early work by Colmenero et al.[19]

The quantitative similarity of the viscoelastic and dielectric mode distributions is not a general feature but specific to the *segmental* relaxation process, as can be easily noted from a significant difference of these distributions for the *global* relaxation of polyisoprene having the type-A dipole (the mode distribution is narrower for the dielectric data than for the viscoelastic data).[42−44] The similarity observed for the segmental relaxation process is discussed later in relation to the motional cooperativity of the segments.

In literature, the dielectric (and viscoelastic) segmental relaxation mode distribution is often fitted by empirical/theoretical equations. For example, the Havriliak−Negami (HN) equation,[45] $\varepsilon^*(\omega) = \varepsilon'(\omega) - i\varepsilon''(\omega) = \varepsilon'(\infty) + \Delta\varepsilon\{1 + (i\omega\tau_{HN})^{\alpha}\}^{-\beta}$ with $i = (-1)^{1/2}$, α and β = constants between 0 and 1, and τ_{HN} = an average characteristic time for intensive relaxation modes, is often utilized to describe the dielectric data in the segmental relaxation zone.[12] However, this equation gives the fractional power-law behavior $\Delta\varepsilon' = \varepsilon''/\tan(\pi\alpha/2) \propto \omega^{\alpha}$ at low ω and $\langle\tau_\varepsilon\rangle = \infty$ (cf. eq 3), which is a contradiction to the experimental observation of the terminal relaxation tails (eq 2) unless $\alpha = 1$. In addition, the fractional power-law behavior associated by the infinite $\langle\tau_\varepsilon\rangle$ is conceptually invalid for our materials (OS, PS) that are in the liquid state and exhibit the full relaxation within a finite time. Thus, the HN equation with $\alpha \neq 1$ (and other similar equations) giving the fractional power-law behavior is just an empirical equation applicable to the data only at around the ε''-peak frequency ω_{peak} and at higher ω. (This behavior is analogous to the behavior of the viscoelastic modulus of critical gels[46] that does not fully relax even at infinitely long time.)

The other equation utilized frequently in literature is the Kohlrausch−Williams−Watts (KWW) equation[28,30,47,48] for the dielectric relaxation function $\varepsilon(t)$

$$\varepsilon_{KWW}(t) = \Delta\varepsilon \exp\left\{-\left(\frac{t}{\tau_{KWW}}\right)^{\beta}\right\} \qquad (4)$$

The dynamic dielectric data are given by the Fourier transformation

$$\Delta\varepsilon'(\omega) + i\varepsilon''(\omega) = i\omega\int_0^{\infty} \varepsilon(t)\exp(-i\omega t)\,dt \qquad (5)$$

The KWW function (eq 4) reproduces the observed terminal relaxation behavior of $\Delta\varepsilon'(\omega)$ and $\varepsilon''(\omega)$ irrespective of the β value, as noted from the low-ω asymptotes analytically calculated from eqs 4 and 5, $\Delta\varepsilon' = \omega^2\Delta\varepsilon\int_0^{\infty}\exp\{-(t/(\tau_{KWW}))^{\beta}\}t\,dt \propto \omega^2$ and $\varepsilon'' = \omega\Delta\varepsilon\int_0^{\infty}\exp\{-(t/(\tau_{KWW}))^{\beta}\}t\,dt \propto \omega$.[48,49] In Figure 11, the circles show the $\varepsilon(t)$ data of the OS and PS samples, $\varepsilon(t) = \Sigma_p g_p \exp(-t/\tau_{\varepsilon,p})$ with the spectrum $\{g_p,\tau_{\varepsilon,p}\}$ obtained from the $\Delta\varepsilon'(\omega)$ and $\varepsilon''(\omega)$ data (Figures 4 and 5) with the aid of the previously reported iteration method.[43] The curves indicate the results of fitting with eq 4. Good fitting was achieved for the dominant part of the relaxation at long t for all OS and PS samples (but not necessarily at short t for some samples). Correspondingly, the $\Delta\varepsilon'$ and ε'' recalculated from the fitted KWW function (with the aid of eq 5) agreed with the $\Delta\varepsilon'$ and ε'' data in the dominant part of relaxation, as shown with the solid curves in Figures 4 and 5. Consequently, the dielectric mode distribution observed for the OS and PS samples is of the KWW-type: This KWW-type mode distribution is often related to a basic, single-τ

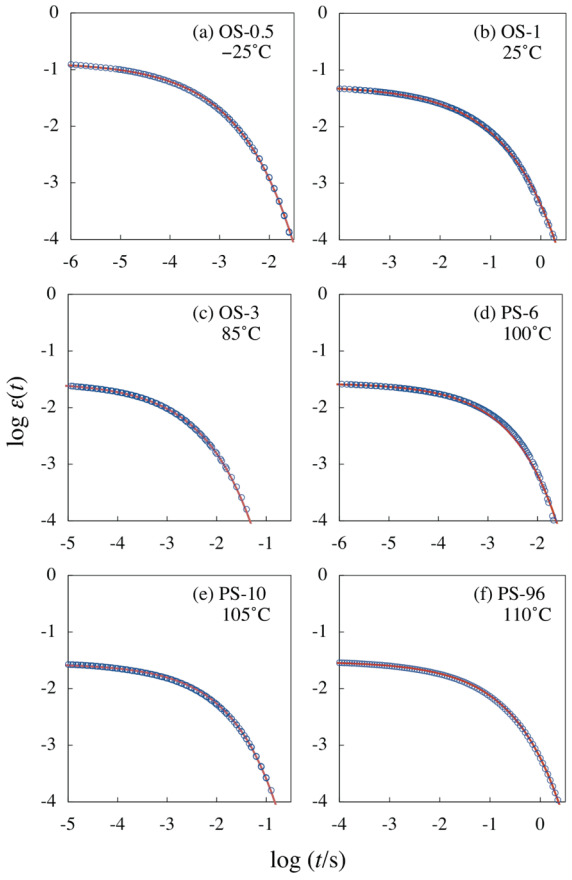

Figure 11. Fitting of the dielectric relaxation function of OS and PS samples (circles) with the KWW function (solid curves).

relaxation process broadened by the intermolecular coupling/correlation as well as the dynamic heterogeneity.[21,28,30]

The KWW parameter representing the mode broadness, β obtained from the fitting in Figure 11, increased a little (from 0.39 to 0.46) with increasing M. Thus, the dielectric mode distribution narrows a little with increasing M, as already explained for Figure 8. However, the change of β is rather minor, confirming that the dielectric mode distribution for the segmental relaxation is rather insensitive to M. (The β values for the PtBS and PLA samples examined in Figure 10, $\beta \cong 0.5$, were close to those for the PS samples.)

The parameter β is often discussed in relation to the intermolecular cooperativity:[2−4,7,9,13,21,28,30] Stronger cooperativity results in smaller β and broader mode distribution. However, in this study, we do not place our focus on the β value because the main finding of this study is the quantitative similarity of the dielectric and viscoelastic mode distributions for the segmental relaxation (Figures 9 and 10). The β value itself does not tell us too much about the molecular origin of this similarity. The similarity of the dielectric and viscoelastic mode distributions is later discussed on the basis of the molecular expressions of the viscoelastic and dielectric relaxation functions.

3.3. Segmental Relaxation Time and Relaxation Intensity. For all OS and PS samples, the terminal relaxation tails of the $\Delta\varepsilon'(\omega)$ and $\varepsilon''(\omega)$ data were observed (cf. Figures 4, 5, and 8), and the relaxation time $\langle\tau_\varepsilon\rangle$ (eq 3) was unequivocally evaluated from those tails with uncertainty less than 40% (which is comparable to usual uncertainty for viscoelastic relaxation time). This $\langle\tau_\varepsilon\rangle$ was close, though not identical, to a characteristic time $\tau_s^{[\varepsilon]} \equiv 1/\omega_{c,\varepsilon}$ defined in terms of the angular frequency $\omega_{c,\varepsilon}$ for the crossing of the $\Delta\varepsilon'$ and ε'' curves, as can be clearly noted in Figures 4 and 5; compare $\omega_{c,\varepsilon}$ and $1/\langle\tau_\varepsilon\rangle$, the latter shown with the arrows. In fact, the $\langle\tau_\varepsilon\rangle/\tau_s^{[\varepsilon]}$ ratio ($\cong 2.5$) was insensitive to the sample molecular weight M, because the dielectric mode distribution determining this ratio hardly changed with M (cf. top panel of Figure 8). This feature, enabling us to utilize $\tau_s^{[\varepsilon]}$ as a *measure* for the terminal dielectric relaxation time consistently for all samples, is very useful for comparison of the dielectric and viscoelastic segmental relaxation times, as explained below.

For the low-M OS-0.5 and OS-1 samples, the moduli $G'(\omega)$ and $G''(\omega)$ were dominated by the segmental dynamics (negligible polymeric contribution) and thus the terminal relaxation tails of the moduli ($G' \propto \omega^2$ and $G'' \propto \omega$) were observed immediately after the viscoelastic segmental relaxation process; see Figures 4a and 4b. For these samples, the terminal viscoelastic time of this process was directly evaluated from those tails as[42] $\langle\tau_G\rangle = [G'/\omega G'']_{\omega\to 0}$ (in a way similar to that for $\langle\tau_\varepsilon\rangle$). The $\langle\tau_G\rangle$ thus obtained was close, though not identical, to the time $\tau_s^{[G]} \equiv 1/\omega_{c,G}$ evaluated from the crossing frequency $\omega_{c,G}$ for the G', and G'' curves, and the $\langle\tau_G\rangle/\tau_s^{[G]}$ ratio ($\cong$2.5) agreed well with the dielectric $\langle\tau_\varepsilon\rangle/\tau_s^{[\varepsilon]}$ ratio (because of the viscoelastic and dielectric mode distributions determining the viscoelastic and dielectric ratios were close to each other; cf. Figure 9). In contrast, for the higher-M samples, the contribution from the polymeric relaxation to the modulus becomes significant so that the terminal relaxation tails of the moduli due only to the segmental relaxation were masked by the polymeric contribution and not accurately resolved; see Figures 4c and 5a−c. However, the viscoelastic mode distribution for the segmental relaxation is similar for the high-M and low-M samples; cf. bottom panel of Figure 8. Because of this similarity, $\tau_s^{[G]}$ evaluated from the crossing frequency $\omega_{c,G}$ can be utilized as a *measure* of the viscoelastic segmental relaxation time *consistently* for both high-M and low-M samples; $\tau_s^{[G]} \cong \langle\tau_G\rangle/2.5$ as noted for the low-M samples. $\tau_s^{[\varepsilon]}$ is utilized as the measure of the dielectric segmental relaxation time in the same sense, as explained earlier. Thus, a difference of the viscoelastic and dielectric segmental relaxation times can be most conveniently/clearly examined for a $\tau_s^{[\varepsilon]}/\tau_s^{[G]}$ ratio: This ratio is equivalent to the $\langle\tau_\varepsilon\rangle/\langle\tau_G\rangle$ ratio for the segmental relaxation and is accurately evaluated from the crossing frequencies $\omega_{c,\varepsilon}$ and $\omega_{c,G}$ (with uncertainties less than 20%).

For all OS and PS samples, Figure 12 shows *double−logarithmic* plots of the $\tau_s^{[\varepsilon]}/\tau_s^{[G]}$ ratio against M. This ratio is affected neither by T nor by T_g of the samples, as can be noted from the coincidence of the viscoelastic and dielectric shift factors at low T (cf. Figures 6 and 7). The $\tau_s^{[\varepsilon]}/\tau_s^{[G]}$ ratio is much larger than unity ($\omega_{c,\varepsilon} \ll \omega_{c,G}$) for small M, decreases significantly with increasing M up to $M^* \cong 2 \times 10^3$, and then becomes independent of M for larger M, as noted in Figure 12. The high-M asymptotic value of the ratio is $\tau_s^{[\varepsilon]}/\tau_s^{[G]} \cong 6$.

This crossover behavior of the $\tau_s^{[\varepsilon]}/\tau_s^{[G]}$ ratio is well correlated with the behavior of the dielectric relaxation intensity $\Delta\varepsilon$. In the top panel of Figure 13, the $\Delta\varepsilon(T_r)$ data of the OS and PS samples at respective T_r are semilogarithmically plotted against M. Since $\Delta\varepsilon$ is inversely proportional to T_r, the $\Delta\varepsilon(T_r)$ data need to be corrected for the difference of the T_r values of the samples. The data after this correction, $\Delta\varepsilon(T_r^o) = \{T_r/T_r^o\}\Delta\varepsilon(T_r)$ with T_r^o = 373 K (100 °C), are shown in the bottom panel. In both panels, we note that $\Delta\varepsilon$ decreases considerably with increasing M up to the crossover molecular weight for the $\tau_s^{[\varepsilon]}/\tau_s^{[G]}$ ratio,

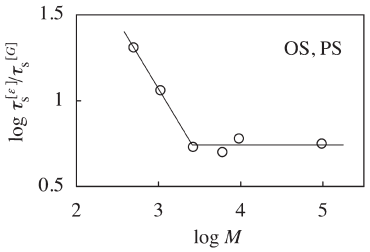

Figure 12. Double−logarithmic plots of the dielectric and viscoelastic segmental relaxation time ratio against OS/PS molecular weight.

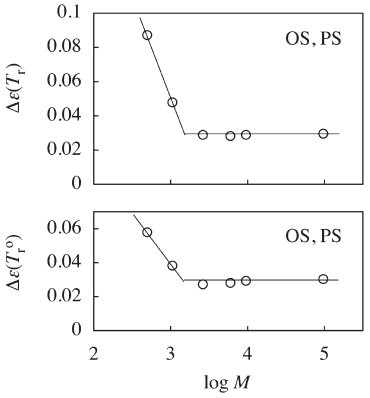

Figure 13. Semilogarithmic plots of the dielectric segmental relaxation intensity against OS/PS molecular weight.

$M^* \cong 2 \times 10^3$, and then becomes independent of M for larger M. These crossover features of the $\tau_s^{[\varepsilon]}/\tau_s^{[G]}$ and $\Delta\varepsilon$ data are discussed below on the basis of the molecular expressions of dielectric and viscoelastic relaxation functions.

4. DISCUSSION

4.1. Molecular Expressions of Dielectric and Viscoelastic Relaxation Functions. Viscoelastically and dielectrically detected segmental relaxation processes of the OS and PS samples are to be discussed on the basis of the molecular expressions of respective relaxation functions. For convenience of this discussion, we introduce unit vectors **n**, **u**, and **v** for each styrene monomer (repeating unit), as schematically shown in Figure 14: **n** is parallel to the monomeric type-B dipole vector (essentially in the direction of the rotational axis of the phenyl group), **u** is parallel to the molecular backbone defined in the direction perpendicular to **n**, and **v** is the normal of the monomeric plane and defined as a vector product, $\mathbf{v} = \mathbf{u} \times \mathbf{n}$.

In the time scale longer than that for the electronic/atomic polarization, the dielectric relaxation function $\varepsilon(t)$ of OS and PS is given by the autocorrelation of microscopic polarization, $\mathbf{P}(t) = \Sigma_p \mu \mathbf{n}_p(t)$, where μ is the magnitude of type-B dipole and $\mathbf{n}_p(t)$ is the unit vector of the pth monomer defined above.[22,23,28−30] Since the motion of the monomers is considered to be cooperative within a characteristic length ξ_c, the autocorrelation $\langle \mathbf{P}(t) \cdot \mathbf{P}(0) \rangle$ includes the cross-correlation of the monomers within a cooperative volume $\sim \xi_c^3$ (the monomers belonging to either the same OS/PS molecule or different molecules) and $\varepsilon(t)$ is expressed as a product of the dielectric intensity $\Delta\varepsilon$ and the

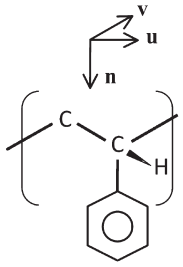

Figure 14. Schematic illustration of unit vectors for styrene monomer in OS and/or PS molecules.

normalized relaxation function $\Phi(t)$[22,23,28−30,50]

$$\varepsilon(t) = \Delta\varepsilon\Phi(t) \tag{6}$$

with

$$\Delta\varepsilon = \frac{\nu g F \mu^2}{3k_B T} \tag{7}$$

and

$$\Phi(t) = \frac{\sum_{p,q}' \langle \mathbf{n}_p^{eq}(t) \cdot \mathbf{n}_q^{eq}(0) \rangle}{\sum_{p,q}' \langle \mathbf{n}_p^{eq}(0) \cdot \mathbf{n}_q^{eq}(0) \rangle} \tag{8}$$

In eq 7, ν is the number density of the monomers, g is the Kirkwood-Fröhlich factor representing the magnitude of motional correlation of the monomeric units (each carrying the dipole), F is a correction factor for the local electric field, k_B is the Boltzmann constant, and T is the absolute temperature. For nonpolar molecules such as OS and PS, F can be expressed in the Onsager form,[30−32,51] $F = (\varepsilon_s + 2)^2/9$ with ε_s being the static dielectric constant. In eq 8, the superscript "eq" stands for the unit vector at equilibrium, the summation $\Sigma'_{p,q}$ is taken for the correlated monomers, and <...> represents the ensemble average.

In the time scale of the segmental relaxation, the styrene monomers behave more or less as planar (slab-like) objects connected in series and the tensile relaxation modulus, $E(t)$ ($\cong 3G(t)$ with $G(t)$ being the shear relaxation modulus), is mainly contributed from the planar (or torsional) orientational anisotropy of the monomers, as revealed from rheo-optical analysis.[26] This $E(t)$ can be compactly expressed in a form,[26]

$$E(t) = Q \sum_p \langle \mathbf{n}_p(t)\mathbf{n}_p(t) - \mathbf{v}_p(t)\mathbf{v}_p(t) \rangle_{zz} \tag{9}$$

In eq 9, Q is an intensity factor representing an increase of the free energy on the planar orientation, and $\mathbf{n}_p(t)\mathbf{n}_p(t)$ and $\mathbf{v}_p(t)\mathbf{v}_p(t)$ indicate the dyadic of the unit vectors of pth monomer under the tensile strain. The subscript zz indicates the diagonal component of the dyadic in the tensile direction (z), and the summation Σ_p is taken for all ν monomers in unit volume. It should be emphasized that $E(t)$ is determined by the orientational anisotropy of individual monomers (represented by the $\langle ... \rangle_{zz}$ term) and detects no cross-correlation of different monomers. This cross-correlation affects the dynamics of $\mathbf{n}_p(t)$ and $\mathbf{v}_p(t)$, thereby implicitly contributing to $E(t)$.

The unit vector $\mathbf{v}_p(t)$ appearing in eq 9 is related to the other vectors as $\mathbf{v}_p(t) = \mathbf{u}_p(t) \times \mathbf{n}_p(t)$. In the time scale of the segmental relaxation, the motion of $\mathbf{u}_p(t)$ is essentially quenched (as noted from the lack of relaxation of rheo-optically detected $\langle \mathbf{uu} \rangle$) so that

eq 9 can be rewritten as

$$E(t) = Q\sum_p \langle \mathbf{n}_p(t)\mathbf{n}_p(t) - \{\mathbf{u}_p \times \mathbf{n}_p(t)\}\{\mathbf{u}_p \times \mathbf{n}_p(t)\}\rangle_{zz} \tag{10}$$

Thus, the time evolution of $E(t)$ is determined by the dynamics of $\mathbf{n}_p(t)$, which is the case also for $\Phi(t)$. However, we should note an important difference: $\Phi(t)$ is contributed from the cross-correlation of $\mathbf{n}_p(t)$ and $\mathbf{n}_q(t)$ of all pairs of different monomers within the correlation volume $\sim\xi_c^3$, while this cross-correlation is *not explicitly* included in $E(t)$.

4.2. Length of Cooperative Sequence of Monomers. The dielectric relaxation intensity $\Delta\varepsilon$ is influenced by the motional correlation of the monomers in the cooperative volume $\sim\xi_c^3$, as represented by the g factor in eq 7. Since the cooperative volume would be very similar for the OS and PS samples at respective $T_r \cong T_g + 20$, the g factor is expected to be insensitive to the molecular weight M of the sample *if* the motional correlation is the same in magnitude for the monomers belonging to the same and different molecules. However, $\Delta\varepsilon$ ($\propto g$) considerably decreases with increasing M up to $M^* \cong 2 \times 10^3$, as seen in Figure 13. This fact strongly suggests that the magnitude of the cross-correlation is different for the monomers in the same and different molecules, as discussed below in more detail.

Since the cooperative volume would be essentially independent of M, the total number of the pairs of the mutually correlated/coupled monomers therein would be also insensitive to M. However, within this volume, the pair number N_{same} for the monomers belonging to the *same* molecule increases while the pair number N_{diff} for those in different molecules decreases with increasing M *given that* the size of the molecule is smaller than the cooperativity length ξ_c; see Figure 15 where the circles indicate the monomers and the connected solid lines show the molecular backbones. Thus, the decrease of $\Delta\varepsilon$ (observed for $M < M^*$) suggests that the cross-correlation is stronger for the monomers in different molecules than for the monomers in the same molecule. This difference is probably attributed to the packing of the monomers around a given monomer: Monomers belonging to different molecules have a much higher freedom in their position/orientation compared to the monomers adjacent to the given monomer in the same molecule. Thus, the monomers belonging to different molecules can be packed with the given monomer more densely to exhibit stronger cross-correlation. On a further increase of $M > M^*$, the size of the molecule exceeds ξ_c so that the pair numbers N_{same} and N_{diff} would become independent of M; see the bottom part in Figure 15. Then, $\Delta\varepsilon$ becomes independent of M, as observed in Figure 13.[52]

From this argument, the cooperativity length, $\xi_c \cong 3$ nm, can be estimated as the size of the OS molecule having $M^* \cong 2 \times 10^3$. This M^* can be regarded as the molecular weight of the cooperative sequence of the monomers in a given molecule exhibiting the torsional motion governed by the intermolecular cross-correlations. We also note that the M^* value corresponds to ~20 styrene monomers, which is in harmony with the traditional molecular picture that the segment of bulk PS corresponds to a sequence of *roughly* 10 monomers.

A comment needs to be made for the above ξ_c value. Since the dielectric and viscoelastic data in the segmental relaxation zone were time−temperature superposed with the same shift factor (cf. Figures 4-7), the ξ_c value deduced from those data is insensitive to T in the range of T examined, mainly between $T_g + 10$ and $T_g + 30$. This time−temperature superposability corresponds to the T-insensitive β value of the KWW function found at T well above T_g.[21] At lower T in the close vicinity of T_g, the superposability should vanish (as expected from a decrease of the β value[21]) and ξ_c would increase accordingly. On the other hand, ξ_c might gradually decrease (and β might gradually increase) in the high T limit ($\gg T_g$) where the intermolecular coupling could become less important. No data are available at such high T, and a further study is desired for ξ_c (and β) in this high-T limit.

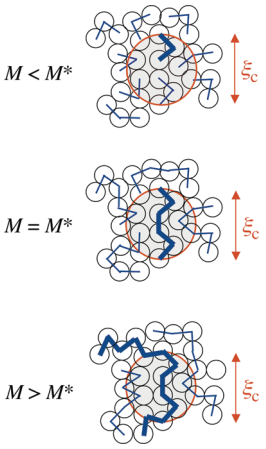

Figure 15. Schematic illustration of cooperative length ξ_c and molecular size. The circles indicate the monomers and the connected solid lines show the molecular backbones.

Now, we focus on the relaxation times of the viscoelastic $E(t)$ and dielectric $\Phi(t)$. The cross correlation, $\langle \mathbf{n}_p\mathbf{n}_q \rangle$ with $p \neq q$, is not explicitly involved in the molecular expression of $E(t)$ (eq 9) but affects the dynamics of $\mathbf{n}_p(t)$ thereby implicitly contributing to $E(t)$. In contrast, the cross-correlation is explicitly included in the expression of $\Phi(t)$ (eq 8) as the main term. Thus, $\Phi(t)$ would be more strongly influenced by the cross-correlation compared to $E(t)$. For a given monomer, the cross-correlation with the monomers in different molecules (within the cooperative volume $\sim \xi_c^3$) is replaced by the weaker cross-correlation in the same molecule on the increase of M up to $M^* \cong 2 \times 10^3$, as suggested from the above argument for $\Delta\varepsilon$. Thus, the relaxation of $\Phi(t)$ dominated by the intermolecular cross-correlation is expected to be accelerated, *in a relative sense*, compared to the relaxation of $E(t)$ thereby decreasing the $\tau_s^{[\varepsilon]}/\tau_s^{[G]}$ ratio on the increase of M up to $M^* \cong 2 \times 10^3$, and this relative acceleration of $\Phi(t)$ would stop for larger M. This expectation is in harmony with the data of the $\tau_s^{[\varepsilon]}/\tau_s^{[G]}$ ratio shown in Figure 12.[50]

In relation to the above results, we note that the asymptotic value of this ratio, $\tau_s^{[\varepsilon]}/\tau_s^{[G]} \cong 6$ for $M > M^*$, is larger than the value expected for a rigid rod-like segment,[39] $\tau_s^{[\varepsilon]}/\tau_s^{[G]} = 3$. This result confirms that the cooperative sequence defined above is not a rigid entity but represents the sequence that can change its shape under the influence of the cross-correlation.

The above M^* value is close to a critical M value, $M_1 \cong 1.8 \times 10^3$, found for a change of the M dependence of T_g of OS/PS reported by Hintermeyer and co-workers.[33] They assigned this M_1 as a critical molecular weight for a crossover from the simple liquid behavior for $M < M_1$ to the Rouse behavior for $M > M_1$ (the crossover not detected for the fragility parameter).[33] The Rouse behavior would emerge only when several torsional cooperative sequences (each having the molecular weight M^*) are connected

dx.doi.org/10.1021/ma200631p |*Macromolecules* 2011, 44, 4355–4365

in series in the molecule. In this sense, there might be an indirect correspondence between their M_1 and our M^* (although M should be much larger than M^* for the Rouse behavior to be observed in a wide range of ω.)

4.3. Similarity of Viscoelastic and Dielectric Mode Distribution of Segmental Relaxation. The cross-correlation of different monomers is explicitly included in the molecular expression for $\Phi(t)$ (eq 8) but not for $E(t)$ (eq 10). Thus, there is no universal/unique relationship between $\Phi(t)$ and $E(t)$. However, for respective OS and PS samples, the relaxation mode distributions of $\Phi(t)$ and $E(t)$ are close to each other, as revealed in Figure 9. This fact indicates that $\Phi(t)$ and $E(t)$ of the OS/PS samples satisfy a specific relationship, $d \ln \Phi(t)/dt = r^{-1}\, d[\ln E(t)]/dt$ with $r = \tau_s^{[\varepsilon]}/\tau_s^{[G]}$.

With the aid of eqs 8 and 10, this relationship can be rewritten in a form that characterizes the dynamics of $\mathbf{n}_p$. However, this rewritten form is obtained for the averaged quantities such as $\langle \mathbf{n}_p^{eq}(t) \cdot \mathbf{n}_q^{eq}(0) \rangle$ and $\langle \mathbf{n}_p(t)\mathbf{n}_p(t) \rangle_{zz}$ and, unfortunately, no explicit Langevin equation of $\mathbf{n}_p(t)$ is deduced from the above relationship. Nevertheless, the quantitative similarity of the viscoelastic and dielectric mode distributions could reflect the coherence of the monomeric motion in the cooperative volume, as expected from analogy with the eigenmode analysis for the global chain motion.[44,53] This coherent motion, including the cooperative torsion of the monomers along the molecular backbone, could be essentially determined by the strong cross-correlation of the monomers belonging to different molecules. (In fact, preliminary experimental results (not shown here) indicated that the viscoelastic mode distribution broadens on dilution of PS with a solvent[54] to deviate from the dielectric mode distribution: This deviation possibly reflects weakening of the intermolecular cross-correlation on dilation and the corresponding reduction of the coherence of motion.) A theoretical study is desired for the similarity of the viscoelastic and dielectric mode distributions for the segmental relaxation in bulk PS as well as for the segmental relaxation time ratio, $\tau_s^{[\varepsilon]}/\tau_s^{[G]} \cong 6$ for high-M PS.

5. CONCLUDING REMARKS

We have examined the viscoelastic and dielectric behavior of OS and PS samples in the segmental relaxation regime. A ratio of the dielectrically and viscoelastically detected segmental relaxation times, $r(M) = \tau_s^{[\varepsilon]}/\tau_s^{[G]}$, and the dielectric relaxation intensity, $\Delta\varepsilon(M)$, were found to decrease with increasing M up to $M^* \cong 2 \times 10^3$ and then became insensitive to M on a further increase of M. This crossover appears to occur when the molecular size exceeds the length scale for the intermolecular cooperative motion of the monomers, and $M^* \cong 2 \times 10^3$ can be assigned as the molecular weight of the cooperative sequence of the monomers along the PS backbone. Furthermore, the quantitative similarity of the viscoelastic and dielectric mode distributions suggests that the cooperative torsional dynamics of the monomers (corresponding to the viscoelastic segmental relaxation) is essentially determined by the cross-correlation of the monomers belonging to different molecules. This molecular picture of dominance of the interchain cross-correlation is expected to be valid also for bulk polymers other than PS, but the characteristic M^* (and the corresponding cooperativity length) may differ from system to system. At this moment, no data are available for the polymers other than PS. A test of this expectation is an interesting subject of our future work.

AUTHOR INFORMATION

Corresponding Author
*E-mail: hiroshi@scl.kyoto-u.ac.jp.

ACKNOWLEDGMENT

This work was supported by the Collaborative Research Program of Institute for Chemical Research, Kyoto University (Grant No. 2011-36), Grant-in-Aid for Scientific Research (B) (Grant No. 21350063), and by Grant-in-Aid for Young Scientists (B) from MEXT (Grant No. 22750204).

REFERENCES

(1) Ferry, J. D. *Viscoelastic Properties of Polymers*, 3rd ed.; Wiley: New York, 1980; Chapter 15.
(2) Kremer, F. Schönhals, A. The Scaling of the Dynamics of Glasses and Supercooled Liquids. In *Broadband Dielectric Spectroscopy*; Kremer, F. Schönhals, A., Eds.; Springer: Berlin, 2003, Chapter 4.
(3) Lunkenheimer, P.; Loidl, A. Glassy Dynamics Beyond the α-Relaxation. In *Broadband Dielectric Spectroscopy*; Kremer, F. Schönhals, A., Eds.; Springer: Berlin, 2003; Chapter 5.
(4) Matsuoka, S. *Relaxation Phenomena in Polymers*; Hanser: Munich, Germany, 1992; Chapter 2.
(5) Donth, E. *J. Non-Cryst. Solids* **1982**, *53*, 325–330.
(6) Fischer, E. W.; Donth, E.; Steffen, W. *Phys. Rev. Lett.* **1992**, *68*, 2344–2346.
(7) Donth, E.; *The Glass Transition: Relaxation Dynamics in Liquids and Disordered Materials*; Springer: Berlin, 2001; Chapters 2 and 3.
(8) Rendell, R. W.; Ngai, K. L.; Mashimo, S. *J. Chem. Phys.* **1987**, *87*, 2359–2362.
(9) Ngai, K. L.; Rendell, R. W.; Plazek, D. J. *J. Chem. Phys.* **1991**, *94*, 3018–3029.
(10) Plazek, D. J.; Ngai, K. L. *Macromolecules* **1991**, *24*, 1222–1224.
(11) Plazek, D. J.; Zheng, X. D.; Ngai, K. L. *Macromolecules* **1992**, *25*, 4920–4924.
(12) Adachi, K.; Kotaka, T. *Prog. Polym. Sci.* **1993**, *18*, 585–622.
(13) Kanaya, T.; Kaji, K. *Adv. Polym. Sci.* **2001**, *154*, 87–141.
(14) Fukao, K.; Sakamoto, A.; Kubota, Y.; Saruyama, Y. *J. Non-Cryst. Solids* **2005**, *351*, 2678–2684.
(15) McKenna, G. B. *J. Phys.-Condensed Matter* **2003**, *15*, S737–S763.
(16) Chen, K.; Schweizer, K. S. *Phys. Rev. E.* **2010**, *82*, 041804.
(17) Cai, W. Z.; Schmidt-Rohr, K.; Egger, N.; Gerharz, B.; Spiess, H. W. *Polymer* **1993**, *34*, 267–276.
(18) McGrath, K. J.; Ngai, K. L.; Roland, C. M. *Macromolecules* **1995**, *28*, 2825–2830.
(19) Colmenero, J.; Alegria, A.; Santangelo., P. G.; Ngai, K. L.; Roland, C. M. *Macromolecules* **1994**, *27*, 407–410.
(20) Schönhals, A. *Macromolecules* **1993**, *26*, 1309–1312.
(21) Cangialosi, D.; Alegria, A.; Colmenero, J. *J. Chem. Phys.* **2009**, *130*, 124902.
(22) Riande, E.; Saiz, E. *Dipole Moments and Birefringence of Polymers*; Prentice Hall: Englewood Cliffs, NJ, 1992.
(23) Watanabe, H. *Macromol. Rapid Commun.* **2001**, *22*, 127–175.
(24) Inoue, T.; Okamoto, H.; Osaki, K. *Macromolecules* **1991**, *24*, 5670–5675.
(25) Inoue, T.; Okamoto, H.; Mizukami, Y.; Matsui, H.; Watanabe, H.; Kanaya, T.; Osaki, K. *Macromolecules* **1996**, *29*, 6240–6245.
(26) Inoue, T.; Matsui, H.; Osaki, K. *Rheol. Acta* **1997**, *36*, 239–244.
(27) Cole, R. H. *J. Chem. Phys.* **1965**, *42*, 637–643.
(28) Schönhals, A.; Kremer, F. Theory of Dielectric Relaxation, in Kremer, F. Schönhals, A., Eds, *Broadband Dielectric Spectroscopy*: Springer: Berlin, 2003, Chapter 1.
(29) Cook, M.; Watts, D. C.; Williams, G. *Trans. Faraday Soc.* **1970**, *66*, 2503–2511.

(30) Riande, E.; Diaz-Calleja, R. *Electrical Properties of Polymers*; Marcel Dekker: New York, 2004.
(31) McCrum, N. G.; Read, B. E.; Williams, G. *Anelastic and Dielectric Effects in Polymeric Solids*; Wiley: New York, 1967.
(32) Runt, J. P.; Fitzgerald, J. J. *Dielectric Spectroscopy of Polymeric Materials: Fundamentals and Applications*; American Chemical Society: Washington DC, 1997.
(33) Hintermeyer, J.; Herrmann, A.; Kahlau, R.; Goiceanu, C.; Rössler, E. A. *Macromolecules* **2008**, *41*, 9335–9344.
(34) Mott, P. H.; Roland, C. M. *Macromolecules* **1998**, *31*, 7095–7098.
(35) Inoue, T; Osaki, K. *Macromolecules* **1999**, *32*, 4725–4727.
(36) Mott, P. H.; Roland, C. M. *Macromolecules* **1999**, *32*, 4728–4728.
(37) One might argue that the complex dielectric permittivity ε^* corresponds to the compliance and thus the complex dielectric modulus $M^* = 1/\varepsilon^*$, rather than ε^*, should be directly compared with the complex viscoelastic modulus G^*. However, M^* reflects the dipolar reorientation processes much less straightforwardly compared to ε^*, and the above argument has no sound molecular basis.[38] An easy example can be found for the dielectric relaxation of rod-like molecules having the dipole parallel to the rod axis. For these molecules, both G^* and ε^* exhibit the single-mode relaxation and the relaxation time τ_G for G^*, directly related to the rotational diffusivity of the molecule, is one-third of τ_ε for ε^* irrespective of the dielectric intensity $\Delta\varepsilon$ determined by the magnitude of dipole.[38,39] M^* also exhibits the single-mode relaxation but its relaxation time, $\tau_M = \tau_\varepsilon/(1+\Delta\varepsilon/\varepsilon_\infty)$ with ε_∞ = unrelaxed high-frequency dielectric constant, depends on $\Delta\varepsilon$.[38] This τ_M decreases (and becomes much smaller than the well-defined τ_G) with increasing magnitude of dipole even if the molecular diffusivity is kept constant. Thus, M^* does not detect the molecular motion straightforwardly and is not suitable for the direct comparison with G^*. Several other examples showing unsuitableness of the direct comparison of M^* and G^* are also known.[38] For this reason, this paper made the direct comparison of the $\Delta\varepsilon^*(\omega)$ $(= \varepsilon^*(0) - \varepsilon^*(\omega))$ and $G^*(\omega)$ data. (This comparison has sound molecular basis,[38] as can be known from the above example of the rod-like molecules.)
(38) Lee, A.; Matsumiya, Y.; Watanabe, H.; Ahn, K. H.; Lee, S. J. *Nihon Reoroji Gakkaishi (J. Soc. Rheol. Jpn.)* **2010**, *38*, 149–155.
(39) Steele, W. A. *Adv. Chem. Phys.* **1976**, *34*, 1–104.
(40) Watanabe, H.; Chen, Q.; Kawasaki, Y.; Matsumiya, Y.; Inoue, T.; Urakawa, O. *Macromolecules* **2011**, *44*, 1570–1584.
(41) Matsumiya, Y.; Inoue, T.; Iwashige, T.; Watanabe, H. *Macromolecules* **2009**, *42*, 4712–4718.
(42) Watanabe, H. *Prog. Polym. Sci.* **1999**, *24*, 1253–1403.
(43) Watanabe, H.; Matsumiya, Y.; Inoue, T. *Macromolecules* **2002**, *35*, 2339–2357.
(44) Watanabe, H. *Polymer J.* **2009**, *41*, 929–950.
(45) Havriliak, S.; Negami, S. *J. Polym. Sci. Part C* **1966**, *14*, 99–1170.
(46) Chambon, F.; Winter, H. H. *J. Rheol.* **1987**, *31*, 683–697.
(47) Williams, G.; Watts, D. C. *Trans. Faraday Soc.* **1970**, *66*, 80–85.
(48) Williams, G.; Watts, D. C.; Dev., S. B.; North, A. M. *Trans. Faraday Soc.* **1970**, *67*, 1323–1335.
(49) Equation 5 can be rewritten in an expansion form, $\Delta\varepsilon'(\omega) + i\varepsilon''(\omega) = -\sum_{n=0}^{\infty}\{(-i\omega)^{n+1}/n!\}I_n$ with $I_n = \int_0^\infty \varepsilon(t)\, t^n\, dt$, if the expansion coverages. The KWW function, $\varepsilon_{KWW}(t) = \Delta\varepsilon \exp\{((-t)/(\tau_{KWW}))^\beta\}$ with $0 < \beta \le 1$, is known to have this expansion form with $I_0 = \Delta\varepsilon\tau_{KWW}\Gamma((\beta+1)/\beta)$ and $I_1 = \Delta\varepsilon\tau_{KWW}^2\Gamma((\beta+2)/\beta)/2$ (Γ = gamma function).[48] Thus, the low-ω asymptotic expression of $\Delta\varepsilon'(\omega)$ and $\varepsilon''(\omega)$ is obtained from the leading terms of the expansion form as $\Delta\varepsilon'(\omega) = I_1\omega^2 \propto \omega^2$ and $\varepsilon''(\omega) = I_0\omega \propto \omega$. Namely, the KWW function gives the terminal relaxation tails (eq 2) irrespective of the β value.
(50) (a) Buchenau [50b] suggested that the dielectric relaxation time of low-M molecules such as glycerol reflects not only the reorientational motion of the molecules but also relaxation of the entropy and density. For the low-M OS samples, the time evolution of the $\langle \mathbf{n}_p^{eq}(t)\cdot\mathbf{n}_q^{eq}(0)\rangle$ term included in eq 8 could be retarded by the entropy/density relaxation. If this entropy/density effect becomes less significant for high-M PS samples, the dielectric relaxation due to the segmental dynamics could be accelerated, *in a relative sense*, compared to the viscoelastic relaxation. This might be an additional mechanism for the crossover of the $\tau_s^{[\varepsilon]}/\tau_s^{[G]}$ ratio seen in Figure 12, although the crossover of the $\Delta\varepsilon$ data does not seem to be well explained by this mechanism. (b) Buchenau, U.; Ohl, M.; Wischnewski, A. *J. Chem. Phys.* **2006**, *124*, 094505.
(51) Onsager, L. *J. Am. Chem. Soc.* **1936**, *58*, 1486–1493.
(52) Schönhals[20] examined the dielectric behavior of *cis*-polyisoprene (PI) having both type-A and type-B dipoles and suggested that the PI chain dimension (end-to-end distance) coincides with the cooperativity length ξ_c when the global relaxation time (detected through the type-A dipoles) coincides with the segmental relaxation time (detected through the type-B dipoles). He evaluated the segmental relaxation time by fitting the data with the Havriliak–Negami equation being invalid in long time scale (as explained in section 3.2 of the current work), which might have affected the ξ_c value he obtained. However, qualitatively speaking, his argument could be somewhat similar to our argument that the effect of the intermolecular correlation on the segmental motion becomes saturated (becomes insensitive to M) when M exceeds the critical M^* value and that ξ_c corresponds to this M^*.
(53) Watanabe, H.; Yao, M. L.; Osaki, K. *Macromolecules* **1996**, *29*, 97–103.
(54) Uno, A.; Watanabe, H.; Inoue, T. Viscoelastic Glass Transition and Local Dynamics of Polystyrene in Solution, *to be submitted to Macromolecules*.